Biomedicine & Pharmacotherapy 141 (2021) 111919

Contents lists available at ScienceDirect

Biomedicine & Pharmacotherapy

journal homepage: www.elsevier.com/locate/biopha

Design and optimization of curcumin loaded nano lipid carrier system using Box-Behnken design

Mukta Agrawal [a], Shailendra Saraf [b], Madhulika Pradhan [a], Ravish J. Patel [c], Gautam Singhvi [d], Ajazuddin [e], Amit Alexander [f,*,1]

[a] Rungta College of Pharmaceutical Sciences and Research, Kohka-Kurud Road, 490 024 Bhilai, Chhattisgarh, India
[b] University Institute of Pharmacy, Pt. Ravishankar Shukla University, Raipur 492 010, Chhattisgarh, India
[c] Ramanbhai Patel College of Pharmacy, Charotar University of Science and Technology, CHARUSAT Campus, Changa, 388 421 Anand, Gujarat, India
[d] Department of Pharmacy, Birla Institute of Technology and Science, Pilani (BITS-PILANI), Pilani Campus, Rajasthan, India
[e] Department of Pharmaceutics, School of Pharmacy & Technology Management, SVKM's NMIMS, Shirpur 425 405, Maharashtra, India
[f] National Institute of Pharmaceutical Education and Research (NIPER-Guwahati), Sila, Changsari, Kamrup, 781 101 Guwahati, Assam, India

ARTICLE INFO

Keywords:
Curcumin
Nano lipid carrier
Alzheimer's disease
Box-Behnken design
Release kinetics

ABSTRACT

Herbal antioxidant like curcumin holds great potential to treat neurodegenerative disease like Alzheimer's disease. However, its therapeutic potency is obstructed due to rapid metabolism, poor solubility, GI susceptibility, enzymatic degradation and lower bioavailability. Thus, the present work aimed to design and optimize curcumin-loaded NLC (CNL) with higher drug entrapment, prolonged release and better stability. CNL was prepared by modified melt emulsification method followed by ultrasonication. The formulation was optimized by 3 factor 3 level Box-Behnken design using solid: liquid lipid, surfactant concentration and ultrasonication time as independent variable while particle size, entrapment efficiency and % drug release as dependant variable. The design suggested 3.092 solid:liquid lipid, 2.131% surfactant and 4.757 min ultrasonication fit best to get the optimized formulation. The size of the optimized CNL was noted 124.37 ± 55.81 nm, which is in the acceptable range for brain delivery. SEM results also comply with this size range (near 150 nm) and demonstrated almost spherical and uniform particles with porous and uneven surface structures. PDI, zeta potential, entrapment efficiency and % drug release were observed as 0.201 ± 0.00, − 17.2 ± 2.35 mV, 93.62 ± 0.68% and 92.73 ± 0.06%, respectively. The NLC demonstrated initial burst release with subsequent prolonged release of drug for 48 h. Weibull kinetic equation with 0.9958 R^2, minimum AIC and maximum MSC value was found best fit to explain the release behavior. The β exponent and diffusional coefficient (n) indicated combined release mechanism with Fickian diffusion as drug release mechanism. Formulation was also found stable at different storage condition.

1. Introduction

Alzheimer's disease (AD) is a progressive neurodegenerative disorder. It is the primary cause of elderly dementia, results in a significant drop in cognitive and memory functions of the brain [1–3]. Advanced health care system and increasing life-expectancy will be supposed to increase the elderly population of the world up to 22% by mid of the century [4]. As per the WHO report, around 50 million people live with dementia, which is expected to multiply by 152 million by 2050. AD contributed 60–70% of all the global dementia cases and became the 6th leading cause of death [5]. Till now, no proper cure is available to treat AD. The existing therapies only relieve the early stage symptoms and not acting on disease pathophysiology to curb its progression [6]. The formation of amyloid β plaque and neurofibrillary tangles are the primary

Abbreviations: AChEI, Acetylcholinesterase inhibitors; AD, Alzheimer's disease; Aβ, Amyloid β peptide; BBB, Blood brain barrier; CNL, Curcumin loaded nano lipid carrier; CNS, Central nervous system; Cur, Curcumin; GI, Gastrointestinal; ICH, International council for harmonization; NLC, Nano lipid carrier; NMDA, N-methyl-D-aspartate receptor; OA, Oleic acid; PBS, Phosphate buffer; PD, Parkinson's disease; PDI, Polydispersity index.

* Correspondence to: Department of Pharmaceutics, National Institute of Pharmaceutical Education and Research (NIPER-Guwahati), Department of Pharmaceuticals, Ministry of Chemicals & Fertilizers, Govt. of India, Sila Katamur (Halugurisuk), Changsari, Kamrup, 781 101 Guwahati, Assam, India.
E-mail addresses: amit.alexander@niperguwahati.ac.in, itsmeamitalex@gmail.com (A. Alexander).
[1] Researcher ID: U-1271-2019; ORCID: 0000-0003-0391-7650; Scopus Author ID: 56794914100

https://doi.org/10.1016/j.biopha.2021.111919
Received 19 May 2021; Received in revised form 3 July 2021; Accepted 12 July 2021
Available online 17 July 2021

pathological factors or hallmark of AD, responsible for the degeneration of neurons [7]. Along with this, dysfunctioning of cholinergic neurons, abnormal functioning of mitochondria, excitotoxicity due to hyperexcitability of NMDA receptors, inflammatory mediators and oxidative stress are other important factors responsible for AD. Genetic abnormalities, environmental factors and exposure to any toxin or chemical also sometimes contribute to the etiology of AD [3,8]. Cholinergic imbalance, oxidative stress, and neuroinflammation seem to be associated with almost all types of AD. Chronic stress condition is one of the most likely risk factors that induce AD [9]. Various studies demonstrated oxidative stress as a crucial factor of AD progression. Outrageous production of free radicles like (reactive oxygen species (ROS)) and decreased function of antioxidant enzymes increases the oxidative stress [10]. It endows AD progression by inducing macromolecular peroxidation, mitochondrial dysfunction and Aβ metal ion redox potency [11]. Unfortunately, the current treatment line involves the clinical use of very few AChEI (acetylcholinesterase inhibitors) like galantamine, donepezil, rivastigmine and an NMDA receptor antagonist like memantine [12,13]. These drug moieties exert symptomatic action and only effective in the early stages of AD. However, to thwart the disease progression, we need a bioactive that directly acts on AD's pathological factors. Various herbal and synthetic molecules [1,14] are under investigation to assess their efficacy against AD.

Among these, **curcumin** is one of the potential candidates extensively explored to treat AD owing to its antioxidant, anti-inflammatory and Aβ plaque degrading ability. Originally it is a polyphenolic compound abundant in rhizomes of *Curcuma longa* L. In general terms, it is known as 'turmeric', native to Southeast Asia particularly, the Indian subcontinent. In Asian and Indian regions, it is a very popular spice used in daily cuisine and an essential part of traditional medicinal systems like 'Ayurveda' [15]. Its potential antioxidant and anti-inflammatory property make it an excellent candidate to treat various inflammatory and degenerative disorders, including cancer, AD, PD etc. Research demonstrated, curcumin impedes the process of amyloidogenesis and obstructs the aggregation of amyloid β peptide in the brain region, hence averts the Aβ plaque formation [16,17]. Alongside, the anti-inflammatory potency of curcumin is attributed to its ability to curb the genetic modulator NF-κB (nuclear factor κB) and lessen the pro-inflammatory cytokines like TNF-α, IL-6 and IL-1β [18]. It also reduces the oxidative stress-induced damage of neurons by attenuation of ROS generation [19]. Owing to such unique therapeutic potentials, curcumin demonstrated considerable improvement in cognitive and memory function of the brain and lessen neurodegeneration [20]. In defiance of its promising therapeutic activities, the clinical application of curcumin is fettered due to poor water solubility, lower bioavailability, rapid clearance, susceptibility to gastrointestinal enzymes and photosensitivity [21]. On contrary, few studies also reported the toxicity of curcumin, for example, Wu et al. observed teratogenic and lethal effect of curcumin at low doses when studied on zebrafish larvae [22]. However, there are a large number of studies and sufficient pieces of evidence available to assure the benefit and safety of curcumin on human usage.

Another notable obstacle in treating neurodegenerative disorders is the existence of protective barrier mechanisms in the brain, the blood-brain barrier (BBB) [23]. Restricting the entry of any foreign material, including the therapeutic agents, is the primary function of the BBB which greatly affects the drug delivery and distribution in the brain [24–26]. In view of this, crossing the BBB or delivering the bioactives across the BBB or bypassing the BBB is the first thing to be considered for the treatment of AD.

Various nanoparticulate systems have been investigated in the past decade to overcome the shortcomings mentioned above of the herbal bioactives and effective delivery to the brain. Among these, lipid-based nanocarriers like solid lipid nanoparticles (SLN) and nano lipid carriers (NLC) offer several advantages over other nanoparticles like higher drug entrapment, biodegradability, biocompatibility, better stability, enhanced cell permeability etc. [27–29]. NLC is known as next generation of SLN or second-generation lipid nanocarrier. Unlike SLN (solid lipid core stabilized with surfactant), NLC is structurally composed of a unique blend of solid and liquid lipid with imperfect lattice arrangement [30]. The imperfect structure provides more space for lodging of drug cargo and hence offers higher entrapment efficiency. It offers significant benefits over SLN also, like better drug loading and entrapment, greater stability, and impedes the expulsion of the drug upon storage. Also, the use of natural lipids or their derivatives makes it higher biocompatible, biodegradable, and less toxic than other nanoparticles [31,32]. NLC significantly improves the solubility of lipophilic drugs and facilitates drug absorption [33]. Alongside, it was found suitable for intranasal delivery of herbal bioactives in previous studies. It overcomes some of the limitations of the nasal route, like enzymatic degradation and poor nasal permeation. It protects the drug from degradation through naso-mucosal enzymes and promotes nasal permeation. Owing to the lower toxicity profile and natural lipid-based composition NLC does not cause any irritation or damage to the nasal mucosa [34].

In view of this, the present research work aimed to design, optimize and characterize an anti-AD drug (curcumin) loaded NLC, which will be further use for direct nose-to-brain delivery. Using this strategy, we tried to eliminate the additional need of targeting or surface-active agents to achieve the goal of cost-effectiveness. All the key elements, including the lipid, drug, and other excipients, are of natural origin. No use of organic solvent during formulation assured the safety of the drug delivery system with minimum possible toxicity or adverse effects.

2. Material and method

2.1. Drug and excipients

Curcumin (Cur, 98%) was kind gift from the Department of Pharmaceutics, Ramanbhai Patel College of Pharmacy (RPCP), CHARUSAT, (Gujarat, India). Glyceryl behenate (Compritol® 888), Glyceryl distearate (Precirol® ATO 5) were provided as gift sample from Gattefosse SAS, France. Glyceryl monostearate (GMS), Glyceryl tristearate (Dynasan® 118), Glyceryl trimyristate (Dynasan® 114), Oleic acid (OA), Triglycerides of capric/caprylic acid (Captex® 300 and Captex® 355), Phospholipon® 80H (70%, soy phosphatidylcholine), Tween 80 and other excipients were also gifted from Department of Pharmaceutics, Ramanbhai Patel College of Pharmacy (RPCP), CHARUSAT, (Gujarat, India). All the other reagents, solvents, and chemicals used in the experiment were of analytical grade.

2.2. Screening of lipids

Solid and liquid lipids for the preparation of CNL were selected on the basis of maximum drug solubility. For solid lipid, the solubility of the drug was tested in GMS, Compritol® 888, Precirol® ATO 5, Dynasan® 118 and Dynasan® 114. One gm of lipid was individually taken in a glass beaker and placed on a magnetic stirrer at a temperature more than 10 ℃ of lipid melting point. Specified amount of drug was gradually added with small increments and constant stirring. Stirring was continued for 30 min upon each addition to assure the complete dissolution of the drug. The mixture was observed for clarity and transparency. The loss of transparency indicated the saturation point of the drug solubility in the lipid.

For selecting liquid lipid, the drug solubility was tested in OA, olive oil, Captex® 355 and Captex® 300. To measure the drug solubility, 5 ml of liquid lipid or oil phase was taken in a glass beaker and kept on magnetic stirrer at room temperature. Precisely weighed amount of the drug was added gradually in the oil/liquid lipid and kept on stirring for 30 min upon each addition. The loss of transparency indicated the saturation point. The resultant solution was then centrifuged (High-speed cooling centrifuge, REMI, C24, India) at 15,000 rpm for 15 min to remove the undissolved drug and supernatant was collected carefully

and analyzed in HPLC (E2695, Water Alliance, USA) to measure the drug content.

2.3. Screening of surfactant

Surfactant was selected on the basis of its impact on the size and stability of the formulation. Different surfactants with varying HLB values were selected for screening. The effect of tween 80 (HLB value 15.0), Transcutol (HLB value 4.2) and Solutol HS15 on the size and stability of blank NLC were measured. The stability was observed by phase separation/creaming or floccule formation in placebo formulation.

2.4. Experiment design (response surface methodology/Box-Behnken design)

Response surface methodology, particularly the three-level, three-factor Box-Behnken design, was used for experimental design and formulation optimization of the preparation of CNL intended for direct nose-to-brain delivery using Design Expert® (Version 10.0.1, State-Ease Inc., Minneapolis, USA). As per the previous literature and formulation variables, the Box-Behnken design found a most suited design for analyzing quadratic response surface and second-order, polynomial model, allowing the process optimization with the minimum possible number of runs (17 runs) including 5 replicated center points. A computer-generated non-linear, polynominal model quadratic equation explaining three-factor three-level design is given below.

$$Y = b_0 + b_1X_1 + b_2X_2 + b_3X_3 + b_{12}X_1X_2 + b_{13}X_1X_3 + b_{23}X_2X_3 + b_{11}X_1^2 + b_{22}X_2^2 + b_{33}X_3^2$$

Where Y stands for dependant variable, b_0 for the intercept, b_1 to b_{33} denotes the regression coefficient calculated from the observations of individual responses and X_1 to X_3 shows the coded levels of prefixed independent variables (X_1 stands for Solid: liquid lipid ratio, X_2 for surfactant concentration and X_3 for ultrasonication time). In addition, the other terms like $X_1 \times_2$, $X_1 \times_3$, $X_2 \times_3$ and X_i^2 (i = 1, 2 and 3) depict the interaction of independent variable and quadratic terms, respectively. The encoded values of various independent and dependent variables, along with their respective levels, are defined in Table 1.

2.5. Preparation of curcumin loaded nanostructured lipid carrier

The CNL (curcumin-loaded nano lipid carrier) was prepared by a modified melt emulsification-ultrasonication technique [35,36]. Initially, Compritol® 888 (melting point, 70 ℃) and Captex® 355 were selected as solid and liquid lipid after lipid screening for the preparation of CNL, respectively. The liquid phase was prepared by melting the solid lipid at a temperature 10 ℃ higher than its melting point. Further, the calculated amount of liquid lipid was added to the melted solid lipid followed by slow addition of the drug with constant stirring to get a clear solution. The aqueous phase containing Tween® 80 (2% w/v) as surfactant and Phospholipon® 80H (1% w/v) as stabilizer was also heated to the same temperature. The aqueous phase was slowly added to the lipid phase at the same temperature with stirring to form a pre-emulsion. This hot pre-emulsion was then subjected to high-speed homogenization (Miccra, D-8 SI, Falc Instruments, Italy) for 3 min to obtain a homogenous mixture. Further, the hot, homogenous pre-emulsion was ultrasonicated using probe sonicator (VCX-500, Vibra-Cell, Sonics & Materials, Inc. USA) for 5 min, pre-set at 550 W with 20:2 on:off cycle. The resulted o/w nanoemulsion was allowed to cool at room temperature to facilitate the formation of CNL by recrystallization of the lipid phase.

The unentrapped drug was removed by centrifugation (High-speed cooling centrifuge, REMI, C24, India) of the aqueous dispersion of CNL. The deposited particles were then redispersed in a sufficient amount of water. Further, mannitol (5% w/v) was added as a cryoprotectant, and the samples were kept for lyophilization (Virtis Advantage EL, Virtis, SP Scientific, Warminster, PA) at 200 torr vacuums for 78 h. The lyophilization produced a very fine, crystallized CNL, which was stored in vials for further experiments (Scheme 1). The formulation and process optimization were carried out using Response Surface Methodology, 3^3 factorial design through Design-Expert®-10 (Version: 10.0.1.0, Stat-Ease, Inc., Minneapolis).

Table 1
Defining different variables and their respective levels of Box-Behnken design for optimization of CNL.

Variables	Levels		
	-1	0	+1
Independent variables			
X1 = Solid: liquid lipid ratio	70:30	75:25	80:20
X2 = Surfactant concentration (%)	1	2	3
X3 = Ultrasonication time (min)	3	5	7
Dependent variables	Constraints		
Y1 = Particle size (nm)	Minimum		
Y2 = Entrapment efficiency (%)	Maximize		
Y3 = Drug release (%)	Maximize		

2.6. Characterization of CNL

2.6.1. Fourier transform infrared spectroscopy (FTIR)

FTIR spectroscopic analysis was performed to investigate the possible interaction and compatibility of drug and lipids used in NLC preparation. The FTIR spectroscopy was conducted by using FTIR spectrometer (Bruker, Massachusetts, USA). Specified amount of sample was mixed with potassium bromide (KBr), and FTIR spectra were observed for pure drug (Cur), physical mixture of drug and lipid and CNL. The scanning was performed in transmission mode, at a wavenumber range from 4000 to 400 cm^{-1}.

2.6.2. Differential scanning calorimetry (DSC)

Thermal properties and phase change behavior of pure drug curcumin, physical mixture of drug and excipients and optimized CNL formulations were analyzed by Differential Scanning Calorimetry (DSC) (Mettler Toledo, DSC3, STAR^e system) associated with the software STAR^e V16.00. Initially, the instrument was calibrated to assure the precision of the result with the help of indium as standard. Accurately weighed amount of samples (2 mg) were packed in 40 μl pin holed standard aluminum pan. The measurement was initiated at 25 ℃ temperature and increases at the rate of 10 ℃/min up to 250 ℃. The sample was analyzed under continuous nitrogen purging at 10 ml/min flow rate during this period. Similar experimental conditions opted for all samples, including the optimized formulation.

2.6.3. XRD

X-ray diffraction pattern of the pure drug Cur, physical mixture and lyophilized CNL was analyzed by PW3050/60 Goniometer based X′pert Pro X-ray diffractometer (Malvern Panalytical Ltd. UK) equipped with Cu anode. Cu-Kα was taken as a radiation source operated at a voltage of 40 kV, a tube current of 30 mA. The samples were scanned at 2θ angle range from 10° to 60° with scan step size 0.026° and continuous scan type.

2.7. Particle size analysis and PDI

The particle size and polydispersity index (PDI) of the prepared CNL formulations were measured by dynamic light scattering technique using particle size analyzer (Malvern ZEN3600, Malvern Panalytical Ltd. UK). The samples were analyzed at room temperature (25 ℃) after diluting the drug-loaded nanocarriers with double distilled water. The particle size and PDI of the diluted samples were measured in triplicate, and the results were reported as an average ± standard deviation.

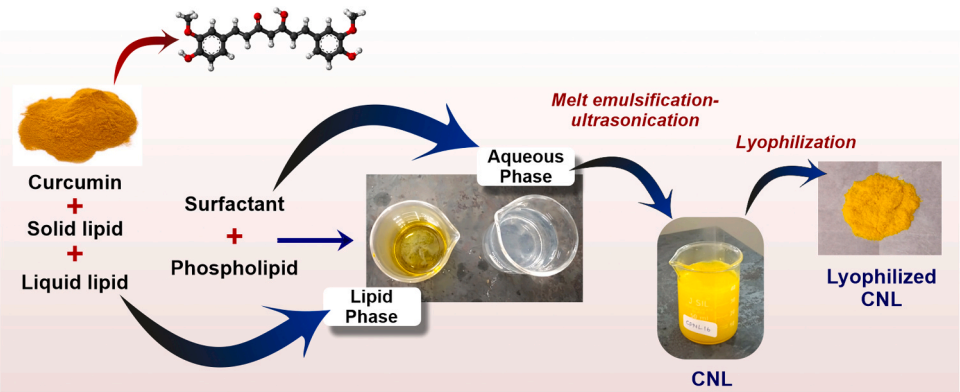

Scheme 1. Schematic representation of formulation of the curcumin loaded NLC.

2.8. Zeta potential

Zeta potential is the measurement of electric charge on the surface of the nanoparticle, which indicates the physical stability of the colloidal carrier system. Zeta potential or surface charge of the prepared CNL was measured by electrophoretic light scattering technique using Zetasizer (ZEN3600, Malvern Panalytical Ltd. UK). The samples were diluted prior to the analysis with doubled distilled water for better signal intensity. The analysis was made in triplicate, and results were reported as mean ± standard deviation.

2.9. Surface morphology through SEM

The surface properties or morphology of prepared CNL were analyzed by scanning electron microscopy (SEM, JSM-6010 LA, JEOL/EO, v1.09 Ltd., Tokyo). The freeze-dried CNL was on an aluminum specimen stub, allowed to dry overnight and gold sputter-coated before scanning. The NLC was examined at 15 kV accelerated voltage.

2.10. % Drug loading and entrapment efficiency

Drug entrapment efficiency is the measurement of amount of drug successfully entrapped into the nanocarrier system. It is calculated with respect to the total amount of drug added during formulation (Eq. (1)). On the other hand, percentage drug loading capacity is the measurement of amount of drug incorporated in the unit weight of the nanocarrier system. It is calculated with respect to the total weight of the formulation (Eq. (2)). Percent drug loading and percent entrapment efficiency of CNL was measured by ultracentrifugation technique using Optima MAX-XP ultra-centrifuge (Beckman Coulter, USA). Appropriate dilutions were prepared by dispersing a specified amount of CNL in distilled water. Prepared aqueous dispersion was filled in the 10 ml centrifugation tube and centrifuged at 55,000 rpm for 30 min at ambient temperature. The supernatant was collected, filtered and the concentration of drug in the supernatant was measured by UHPLC (Thermo Fisher Scientific, MA, USA, equipped with FLD detector). Further, the % drug loading and % entrapment efficiency were calculated by using the following formulas.

$$\%\ Entrapment\ Efficiency = \frac{Total\ amount\ of\ drug - amount\ of\ free\ drug}{Total\ amount\ of\ drug} \times 100 \quad (1)$$

$$\%\ Drug\ Loading = \frac{Total\ amount\ of\ drug - amount\ of\ free\ drug}{Total\ amount\ of\ NLC} \times 100 \quad (2)$$

2.11. In vitro release study

The in vitro drug release of lyophilized CNL was conducted by dialysis membrane method using Franz Diffusion cell assembly (25 ml capacity and 2.0 cm diameter). The dialysis membrane with mol. wt. cut-off between 12 and 14 kDa was selected as diffusion membrane, and phosphate buffer (PBS) pH 7.4 was used as dissolution media. Prior to the experiment, the dialysis membrane was cut into pieces of desirable size and treated with the dissolution medium by soaking in PBS, pH 7.4 for 48 h. The receptor compartment of the assembly was filled with PBS, pH 7.4 and the open end was mounted with pre-treated dialysis membrane. The sample was prepared by dispersing specified amount of lyophilized powder of optimized batch of CNL (equivalent to 2.0 mg of curcumin) in buffer solution. The lyophilized sample was preincubated at 37 ℃ for 20 min before use. On the other hand, the drug solution was prepared by dissolving 2.0 mg of curcumin in the buffer using ethanol as cosolvent. Both the test samples were filled in separate donor compartments. The assembly was maintained at 37 ℃ temperature throughout the study. Periodic sampling was done from the receptor compartment and replaced with equal amount of fresh medium. Finally, the samples were analyzed by UHPLC (Thermo Fisher Scientific, MA, USA, equipped with FLD detector) to determine the drug concentration.

2.12. Stability study

Accelerated stability study was conducted as per ICH guidelines Q1A (R2) by incubating the prepared optimized batch of CNL at regular (25 ± 2 ℃ temperature and 60 ± 5% RH) and accelerated conditions (40 ± 2 ℃ temperature and 75 ± 5% RH) for 3 months. The stability was measured in terms of physical appearance, particle size and % entrapment efficiency of the formulation. The effect of temperature and humidity was observed in specific time period; 0 month, 1 month and 3 months [37,38].

2.13. Statistical analysis

All the experiments were performed in triplicate, and the values reported were the average of three measurements with standard deviation (± SD). Statistical assessments were carried out by comparison among various groups of study using ANOVA for the analysis of variants. Design Expert® (Version 10.0.1, State-Ease Inc., Minneapolis, U.S.A.) and DDSolver 1.0 (Microsoft Corp., U.S.A.) were used for statistical analysis of different parameters. P-value < 0.05 was considered significant.

3. Results

3.1. Screening of lipid and surfactant

The screening of solid and liquid lipid by solubility and compatibility suggested Compritol® 888 ATO and Captex® 355 as the most suitable and compatible solid and liquid lipid for the preparation of drug-loaded NLC. Curcumin showed maximum solubility in melted Compritol® 888 ATO. The selected lipids demonstrated desired stability and found safe with mucus layer and different cell lines [39,40]. Surfactant was selected on the basis of its impact on the size and stability of the NLC, and after screening, we found Tween 80 as the best-suited surfactant for the present study.

3.2. Physicochemical characterization

3.2.1. FTIR

FTIR spectra of the pure drug, physical mixture of drug and excipients and final lyophilized product were performed to study the possible interaction between the drug (curcumin), lipid and other excipients used in the formulation. The FTIR spectra of Cur, physical mixture of Cur, lipids and other excipients and lyophilized CNL is shown in Fig. 1. Fig. 1 (a) shows the FTIR spectra of pure drug, which showed all the characteristic peaks of curcumin. A medium intensity peak at 1627.64 cm^{-1} and 1602.64 cm^{-1} represented characteristic overlapped stretching vibration of C═O (carbonyl) group and C═C (alkene), respectively. The absorption band at 3508.08 cm^{-1} stands for phenolic-OH stretching vibration. Strongest peak observed in the finger printing region at 1509.89 cm^{-1} indicated mixed vibrational band due to in-plane bending vibration of aliphatic C—C, C—O as well as C—H keto-enol configuration of curcumin. Stretching vibration of C═C olefinic observed at 1428.25 cm^{-1}. Additionally, medium intensity at 1281.26 cm^{-1} represented C—O—C stretching. C—H stretching of aromatic, aliphatic and C═C (olefinic) are observed at 3070.12 cm^{-1}, 2917.23 cm^{-1}, and 3070.12 cm^{-1} respectively. Fig. 1(b) shows the FTIR spectra of physical mixture of curcumin and Compritol® 888/Glyceryl behenate (lipid). High-intensity peak at 2919.27 cm^{-1} and 2851.89 cm^{-1} represented characteristic C—H stretching vibration of long-chain alkane (Glyceryl behenate) and C—H stretching vibration C═C (curcumin), respectively. While peak at 1468.39 cm^{-1} is due to C—H bending vibration of alkane. C═O stretching of aliphatic ester observed at 1724.64 cm^{-1}. —OH stretching of long-chain aliphatic alcohol observed at 3389.22 cm^{-1}. Peak at 1175.16 cm^{-1} is due to C—O stretching vibration of saturated ester. A characteristic rocking vibration of long-chain CH2 group arises at 723.03 cm^{-1}. Fig. 1(c) FTIR spectra of CNL: High-intensity broad peak at 3455.85 cm^{-1} is due to high concentration of free OH group of both curcumin and Glyceryl behenate. C—H stretching of aliphatic 2916.55 cm^{-1}. While peak at 1452.71 cm^{-1} is due to C—H bending vibration of alkane. Intense broad peak arises at 1640.40 cm^{-1} is due to overlap of C═O stretching vibration of curcumin and Glyceryl. The formation of NPs is confirmed by shifting of characteristic peak C═O of Glyceryl behenate from 1724.64 cm^{-1} to 1640.40 cm^{-1} in NPs.

3.2.2. DSC

DSC analysis of the prepared nanoformulation was carried out as a standard technique to study the phase transition properties and effect of thermal changes on the crystallinity and physical state of the sample. A comparative assessment between the pure drug, lipid, physical mixture and drug-loaded lipid nanocarrier confirms the characteristics of the pure drug and lipid. Also, it provides a clear idea about changes in drug properties upon loading into the nanocarrier. DSC thermogram of the pure drug curcumin, lipid phase Compritol® 888 ATO, physical mixture and lyophilized CNL is shown in Fig. 2. The thermogram of Cur showed a sharp, endothermic peak at 177.06 ℃, indicating the melting point of the drug. The sharp endothermic peak of COMP at 72.85 ℃ showed the melting point of the solid lipid (Compritol® 888 ATO) and is very much similar to the reported melting point values in standard monographs. The thermogram of physical mixture of CNL has a clear, sharp, endothermic peak of Compritol® 888 ATO while the endotherm of Cur disappeared. Likewise, the lyophilized CNL has the characteristic peak of lipid and missing the melting endotherm of the drug. The disappearance of peak and change in the thermal property of Cur in the physical mixture and lyophilized CNL might be attributed to complete solubilization or molecular dissolution of the drug in the lipid phase [36,41,42]. The disappearance of cur peak also supports the previous finding of the solubility of the drug in Compritol® 888 ATO and assures complete and higher entrapment in nanocarrier systems [43].

3.2.3. XRD

XRD pattern was used to analyze the crystalline behavior of the pure drug, physical mixture of drug and lipid and the drug-loaded NLC (Fig. 3). The sharp, high-intensity peaks in the diffractogram resulted from the presence of highly crystalline lipid content, while the low-intensity peaks represent the amorphous lattice structure. Natural lipids and their derivatives with the composition of mono-, di-, triglycerides and fatty acid esters like Compritol®, Precirol, Captex® etc., form imperfect crystalline structures and resulted in higher drug entrapment by providing extra space for the accommodation of drug molecules. Fig. 3(a) shows the sharp, high-intensity peaks at 2θ scattered angles of 17.4, 19.6, 21.7, 23.9, 24.7, 25.7, 26.1, 27.5 etc., which are characteristics of the drug curcumin, showing its crystalline nature. In Fig. 3(b), the physical mixture of drug and lipid, high-intensity peaks were observed only near the scattered angle of 19.6, 23.7 and 21.5. The decreased peak intensities observed in the physical mixture resulted from the reduction of crystalline behavior of the curcumin. At the same time, the lyophilized CNL showed some high-intensity characteristic peaks of the drug due to the presence of curcumin at the outer layer of the lipid matrix. Besides, the reduction of the high-intensity peaks showed the entrapment of drugs in the lipid matrix, which is amorphous in nature. The combination of low and high-intensity peaks in the diffractogram of lyophilized CNL (Fig. 3(c)) showed the imperfect lattice structure of the lipid nanocarrier with a massive crystalline arrangement. Such imperfect arrangement of lipid offers higher space for drug entrapment and thus enhances the drug entrapment efficiency. The XRD pattern also demonstrated molecular dispersion of curcumin in the lipid matrix, enhancing the solubility of the drug.

3.3. Data analysis and formulation optimization

Three factors and three-level Box-Behnken design was used for experimental design and process optimization. The response surface randomized design results in 17 runs of different combinations of the chosen factors, including 5 runs with central points for which the responses were recorded and analyzed. The specific model terms found best fitted for all three factors are quadratic polynominal models. The model terms denoted a direct effect of independent variables on the dependent variables (responses). All the observed responses were comparatively assessed to identify the best experimental parameter. The analysis of the responses was performed by using ANOVA (analysis of variants) to predict the best mathematical model and optimized parameters. Coefficient and p-values of individual and combined factors indicated the influence of respective factors on selected responses. P-value also displayed the significance of the applied model and other parameters assessed by ANOVA (Table 3). As desired, the model terms found significant, and lack of fit was not significant for each observed response. The 17 runs of experimental design and respective responses of individual runs are shown in Table 2. The 3D response surface plots of all the responses showing the effects of different factors are presented in Fig. 4. Final regression equation of the applied quadratic model for individual responses, including particle size (Y_1), drug entrapment efficiency (Y_2) and drug release (Y_3) produced by response surface methodology using DesignExpert® software are given below.

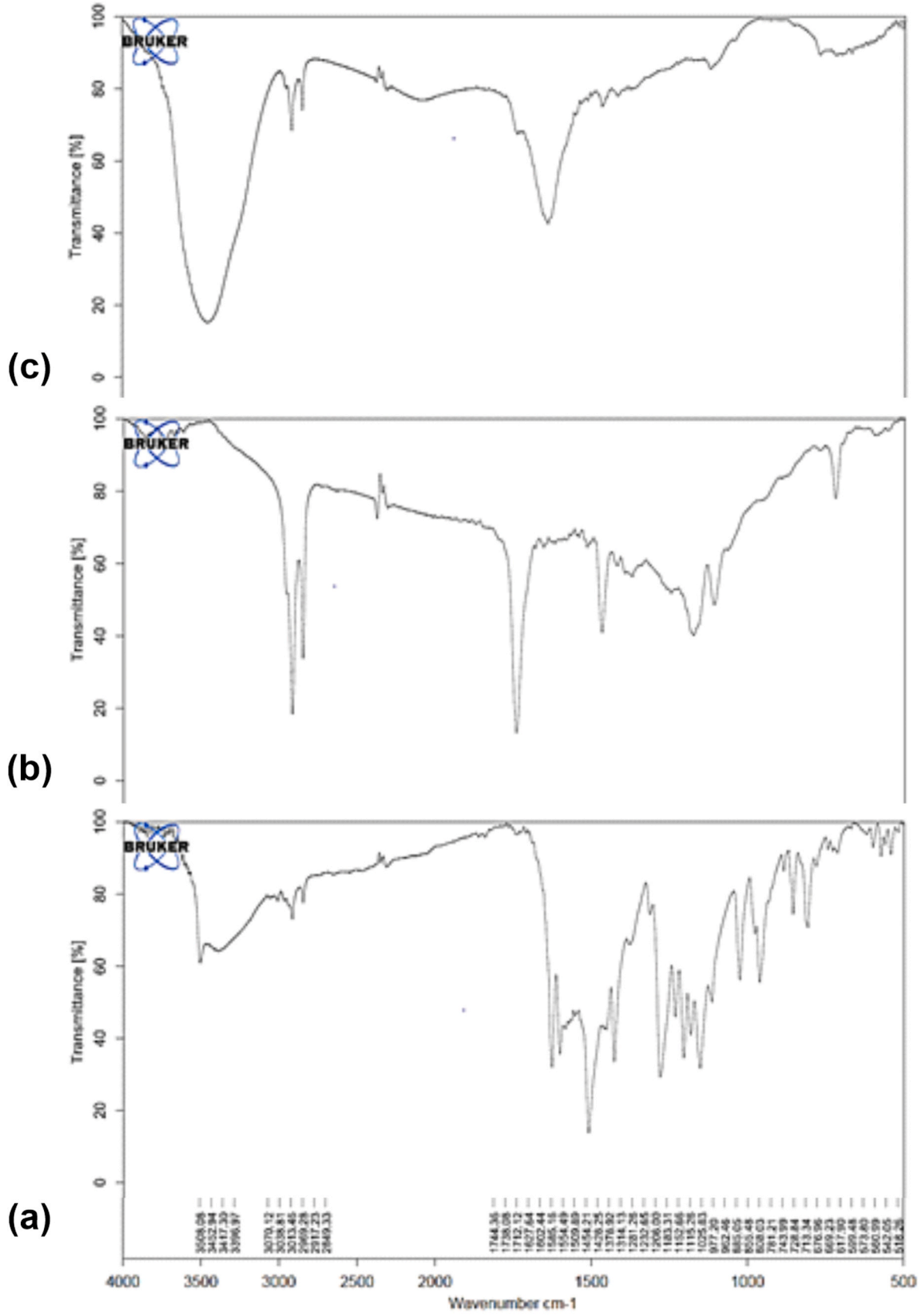

Fig. 1. FTIR spectra of (a) pure drug curcumin, (b) physical mixture of drug and lipid and (c) lyophilized CNL.

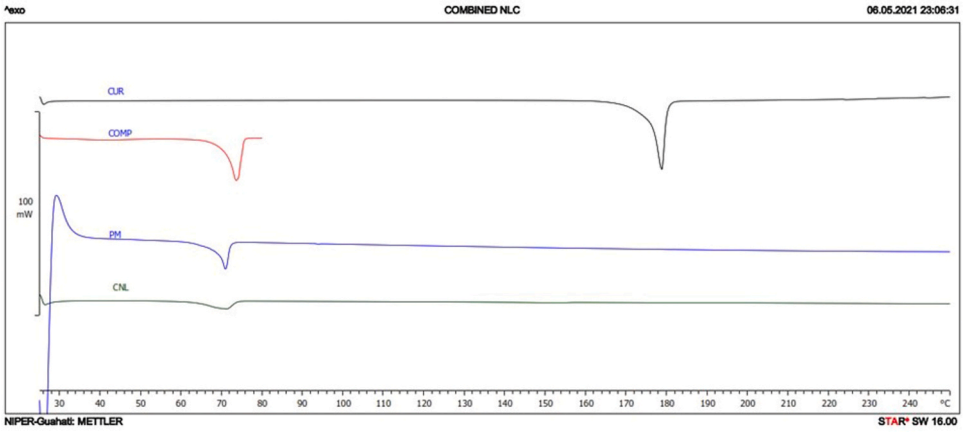

Fig. 2. DSC thermogram of the plain drug curcumin (CUR), lipid Compritol® 888 ATO (COMP), physical mixture (PM), and lyophilized sample of curcumin loaded NLC (CNL).

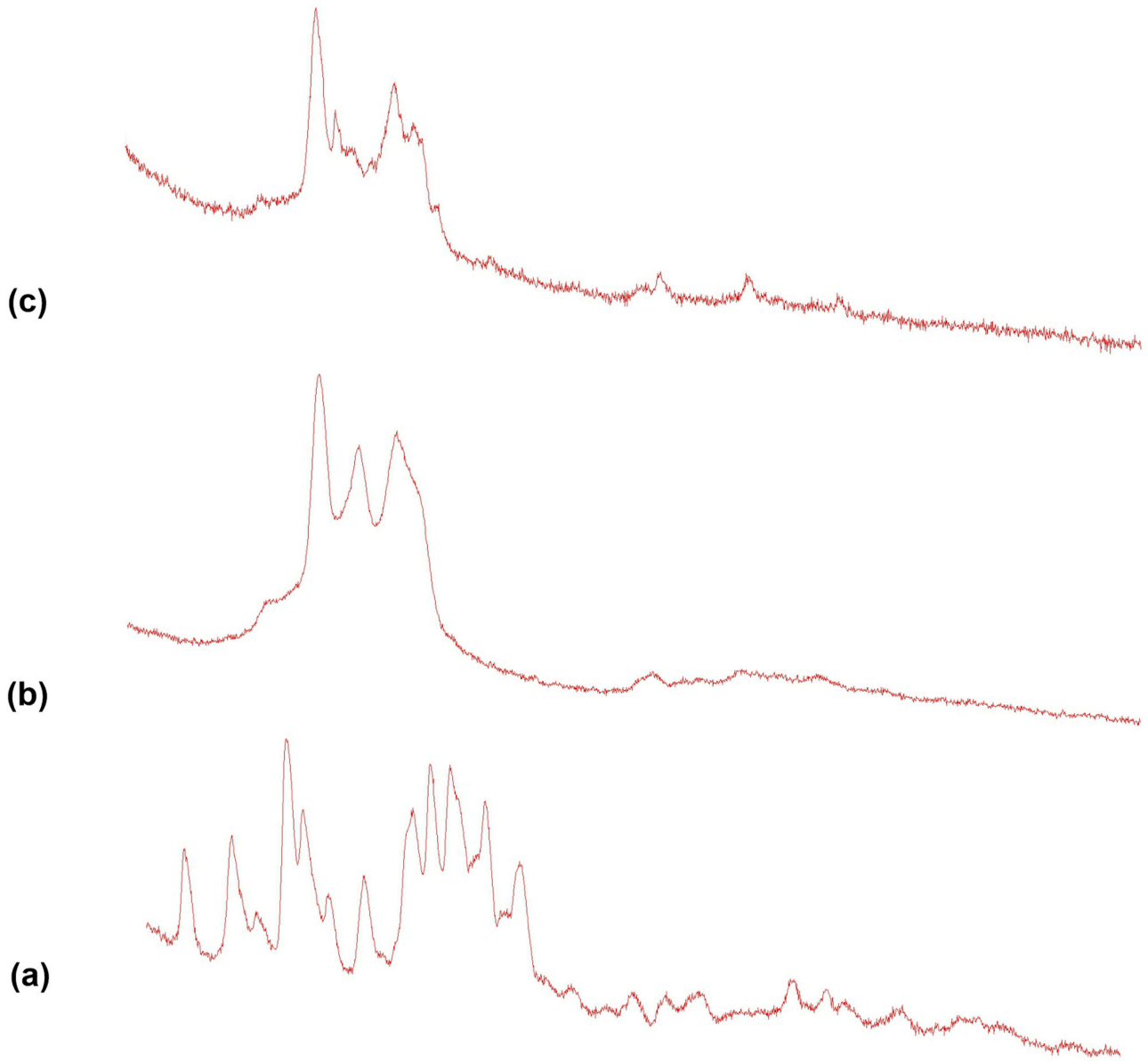

Fig. 3. XRD pattern of (a) pure drug curcumin, (b) physical mixture of drug and lipid and (c) lyophilized CNL.

Table 2
Effect of various formulation variables (independent factors) on the characteristic features of the prepared CNL using response surface methodology Box-Behnken design for optimization of the formulation.

Batch code	Factor A Solid: Liquid lipid ratio X1	Factor B Surfactant Concentration X2 (%)	Factor C Ultrasonication Time X3 (min)	Response 1 Particle size Y1 (nm)		Response 2 Entrapment Efficiency Y2 (%)		Response 3 Drug Release Y3 (%)	
				Actual	Predicted	Actual	Predicted	Actual	Predicted
CNL1	0	0	0	70.92	121.052	91.57	91.68	92.56	90.9962
CNL2	0	1	1	203.79	220.194	66.33	68.58	72.38	72.1925
CNL3	0	0	0	177.69	121.052	93.70	91.68	90.521	90.9962
CNL4	-1	-1	0	377.86	405.908	81.62	80.86	66.39	66.0155
CNL5	0	-1	-1	320.97	304.567	78.54	76.29	68.41	68.5975
CNL6	0	-1	1	334.63	331.994	66.09	68.45	65.374	62.5155
CNL7	-1	0	-1	246.50	234.851	71.46	74.48	69.48	69.667
CNL8	0	0	0	86.09	121.052	88.62	91.68	92.73	90.9962
CNL9	0	0	0	136.42	121.052	91.35	91.68	87.38	90.9962
CNL10	0	1	-1	244.46	247.093	76.05	73.69	74.64	77.4985
CNL11	1	0	1	306.03	317.677	78.63	75.61	70.43	70.243
CNL12	-1	0	1	297.05	271.633	73.67	72.08	67.21	70.443
CNL13	1	0	-1	328.51	353.931	84.57	86.16	85.64	82.407
CNL14	1	-1	0	395.14	386.12	78.76	79.42	67.51	70.5555
CNL15	-1	1	0	209.90	218.921	71.24	70.58	76.62	73.5745
CNL16	0	0	0	134.15	121.052	93.17	91.68	91.79	90.9962
CNL17	1	1	0	431.88	403.833	86.46	87.22	81.2	81.5745

Table 3
Summary of ANOVA and statistical parameters respective to selected responses indicating significance and fitting of different models.

Model fit parameters	Y_1: Particle size		Y_2: Entrapment Efficiency		Y_3: Drug release	
	p-value	Interpretation	p-value	Interpretation	p-value	Interpretation
Model	0.0016	Significant	0.0007	Significant	0.0006	Significant
R^2	0.9405	–	0.9537	–	0.9560	–
R^2_adjusted	0.8640	–	0.8941	–	0.8994	–
AICc	215.25	–	127.01	–	130.28	–
Lack of fit	0.6000	Not significant	0.1095	Not significant	0.1122	Not significant
X_1	0.0224	Significant	0.0087	Significant	0.0307	Significant
X_2	0.0202	Significant	0.5766	Not significant	0.0052	Significant
X_3	0.9928	Not significant	0.0181	Significant	0.0441	Significant
X_1X_2	0.0376	Significant	0.0191	Significant	0.6149	Not significant
X_1X_3	0.3917	Not significant	0.2142	Not significant	0.0897	Not significant
X_2X_3	0.5190	Not significant	0.6605	Not significant	0.9093	Not significant
X_1^2	0.0004	Significant	0.0512	Significant	0.0022	Significant
X_2^2	0.0009	Significant	0.0005	Significant	0.0003	Significant
X_3^2	0.0438	Significant	0.0001	Significant	0.0004	Significant

$$Y_1 = 121{\cdot}05 + 41{\cdot}28 \times_1 - 42{\cdot}32 \times_2 + 0.13 \times_3 + 51{\cdot}17\ X_1X_2 - 18{\cdot}26\ X_1X_3 - 13{\cdot}58\ X_2X_3 + 125{\cdot}60 \times_1^2 + 107{\cdot}04 \times_2^2 + 47{\cdot}87 \times_3^2 \quad (3)$$

$$Y_2 = 91{\cdot}68 + 3{\cdot}80 \times_1 - 0.62 \times_2 - 3{\cdot}24 \times_3 + 4{\cdot}52\ X_1X_2 - 2{\cdot}04\ X_1X_3 + 0.68\ X_2X_3 - 3{\cdot}42 \times_1^2 - 8{\cdot}75 \times_2^2 - 11{\cdot}18 \times_3^2 \quad (4)$$

$$Y_3 = 91{\cdot}00 + 3{\cdot}14 \times_1 + 4{\cdot}64 \times_2 - 2{\cdot}85 \times_3 + 0.86\ X_1X_2 - 3{\cdot}23\ X_1X_3 + 0.19\ X_2X_3 - 7{\cdot}54 \times_1^2 - 10{\cdot}53 \times_2^2 - 10{\cdot}27 \times_3^2 \quad (5)$$

The response surface plot and coefficient of the quadratic equation clearly indicated that the selected factors significantly impact the dependent variables (Y_1, Y_2, and Y_3). The positive and negative signs before individual terms of the regression equation showed the increase and decrease in the response with the factors, respectively.

3.3.1. *Effect of independent factors on Response Y_1 (Particle size)*

Results showed that particle size of all the prepared formulations ranges from 70.92 nm to 431.88 nm. As per the regression equation, it was very much clear that particle size (Y_1) was directly affected by the lipid ratio (solid: liquid lipid) (X_1), while inversely related to the surfactant concentration (X_2), and there is no significant effect of ultrasonication time (X_3), Eq. (3). 3D response surface plot provides more detailed information on the effect of various independent factors on particle size (Fig. 4(A)–(C)). The graph showed initial decrease in particle size with a shift of solid/liquid lipid ratio (X_1) from the level − 1 to 0 followed by significant increases with further increase from 0 to + 1. This response might be due to an initial increase in the solid lipid will provide a perfect blend of solid and liquid lipid, resulting in the desired structure of NLC with minimum possible size. In contrast, further increase in solid lipid concentration increases accumulation of solid content and hence the particle size. In addition, an increase in surfactant concentration (X_2) initially resulted in a considerable decrease followed by slight increase of particle size with further rise of surfactant concentration. Initial increase in surfactant concentration supposed to reduce the interfacial tension and create steric hindrance on NLC surface to prevent the accumulation of individual particles and improve stability [44]. Once the surfactant concentration reaches saturation point, further increase cause deposition of excess surfactant molecules on the NLC surface and again result in slight rise of size. Ultrasonication time did not exert significant effect on the particle size. Very slight changes were observed with increasing ultrasonication time, and minimum particle size was found at the center point value. It was clear from the 3D plot that the interaction of factors A and B and factors A and C synergistically affect the particle size. Maximum particle size was observed with highest level of X_1 and X_2, while minimum size was found with center value of all the independent factors.

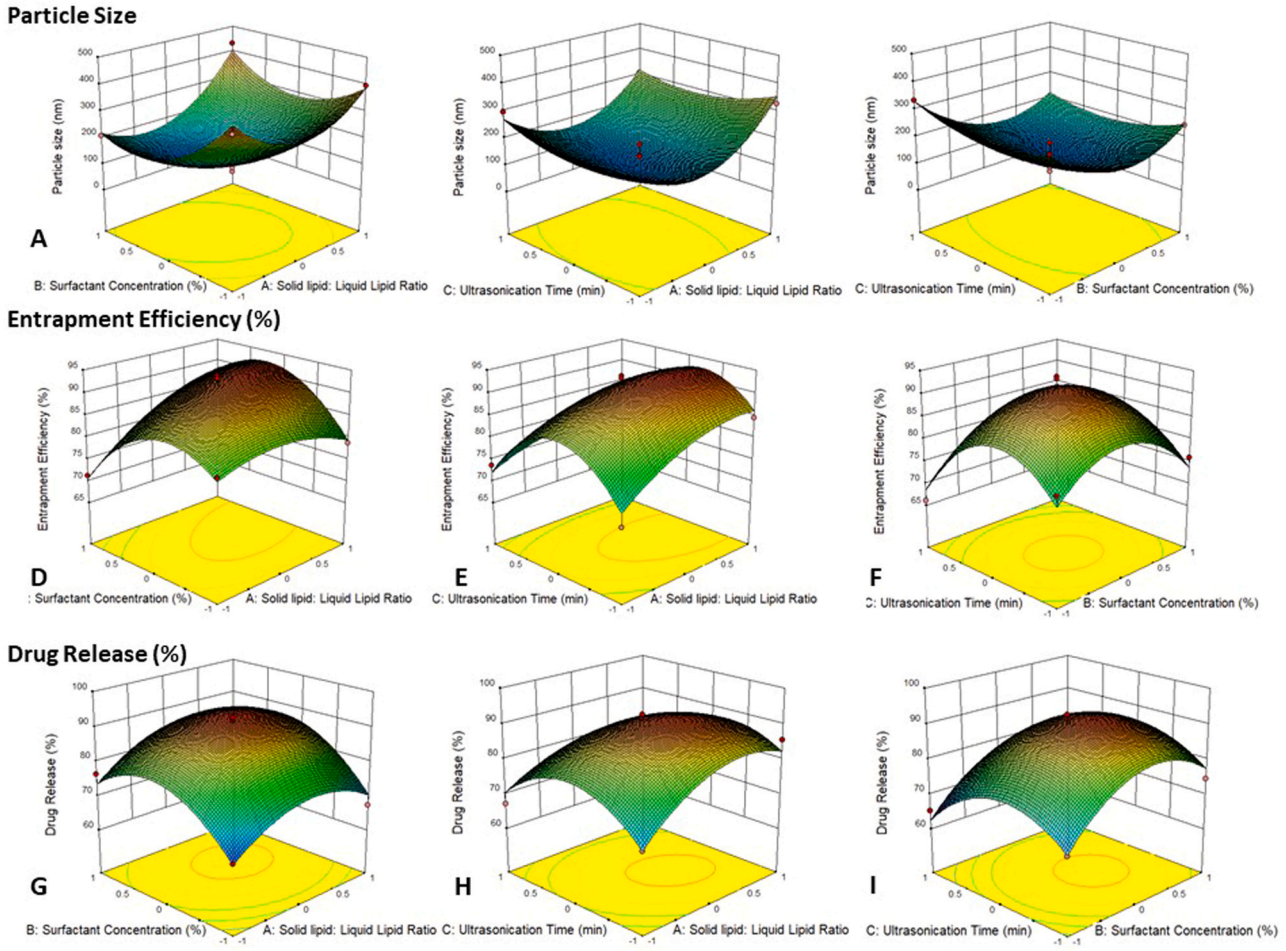

Fig. 4. 3D-response surface plot for optimization of the prepared formulations, showing the impact of different formulation variables (independent factors) on characteristic features of the developed NLC; (A–C) effect of X1, X2 and X_3 and their interaction terms on particle size (Y_1); (D–F) effect of X1, X2 and X_3 and their interaction terms on entrapment efficiency (Y_2); and (G–I) effect of X1, X2 and X_3 and their interaction terms on particle size (Y_3).

3.3.2. Effect of independent factors on Response Y_2 (Entrapment Efficiency)

The % entrapment efficiency of the prepared formulations was found between the range of 66.09–93.70%. The final quadratic equation indicated that the entrapment efficiency of the formulation is directly proportional to the lipid ratio while inversely proportional to the surfactant concentration and ultrasonication time, Eq. (4). The 3D response surface plot showed significant enhancement in % entrapment efficiency with increasing solid/liquid lipid ratio followed by slight decline with further increase. This might be due to the initial increase in solid lipid content facilitate solubilization of drug (as curcumin has good solubility in melted Compritol® 888). Further increase in lipid ratio resulted in excessive reduction of liquid lipid content, which minimized the liquid compartment of drug entrapment in the NLC matrix and promoted the expulsion of already entrapped drug from the solid matrix. Likewise, an increase of surfactant concentration and ultrasonication time initially resulted in a growing curve of entrapment efficiency followed by subsequent decline with further improvement. An increase in surfactant concentration could enhance the drug partitioning and facilitate its solubilization in both the lipid and aqueous phases [45]. The lipid matrix might get saturated with a further increase of surfactant, and a reduction of entrapment efficiency was observed due to the drug expulsion from the lipid matrix. On the other hand, the application of high energy agitation during ultrasonication assisted the movement of drug molecules from the aqueous phase to the lipid matrix and increases the drug entrapment, while further increase in sonication time may cause expulsion of the loosely bound drug from the matrix (Fig. 4(D–F)). Maximum drug entrapment was observed with the center point values of the interaction terms X_1X_2, X_1X_3 and X_2X_3.

3.3.3. Effect of independent factors on Response Y_3 (% Drug Release)

All the formulation variables or independent factors have a considerable impact on the % drug release of the Cur loaded NLC. % drug release of the developed formulations may vary from 65.37% to 92.73%. The coefficient values of individual factors showed a direct effect of lipid ratio and surfactant concentration while inverse effect of ultrasonication time on the % drug release of the CNL. Impact of independent variables were described by quadratic Eq. (5). In the response surface plot, first increase and then decrease was observed with increasing lipid ratio. In a similar manner, initial increase was noted with an increase in surfactant concentration and ultrasonication time, but further, both factors led to a decrease in drug release (Fig. 4(G–I)). These responses were also in line with the effects of individual factors on entrapment efficiency. As the formulations prepared with center point values of independent factors had higher amounts of drug entrapped in the lipid matrix, maximum release was also evident with that ratio.

3.3.4. Optimization and point prediction

After statistical analysis and assessment of the impact of individual factors on the responses, the optimization of the prepared formulations was done by the software. Optimization gives precise formulation parameters to achieve the desired goals of the selected responses. As per

the desirability, particle size (Y_1) was set to minimize, entrapment efficiency (Y_2) and drug release (Y_3) were set to maximize. The numerical optimization of the Box-Behnken design suggested most suitable values of the formulation variables as 3.092 solid: liquid lipid ratio, 2.131% surfactant concentration and 4.757 min ultrasonication time. The predicted responses for optimized formulation by DesignExpert® were noted as 123.964 nm, 92.067% and 91.887% for particle size, entrapment efficiency and drug release, respectively. Further, the finally optimized batch was prepared as per the suggested proportion and experimental conditions, which was then subjected for further evaluation.

3.4. Particle size, PDI and zeta potential

The response depicted a direct effect of solid lipid concentration on the size of NLC formulation. The result showed an increase in particle size with increasing ratio of solid and liquid lipid, i.e., increasing concentration of solid lipid while vice versa was observed with reducing ratio of lipids. In addition, surfactant concentration also significantly impacts the size of CNL (as discussed earlier). The final batch was prepared and analyzed for particle size, PDI and zeta potential through dynamic light scattering based on design optimization. We observed particle size 121.8 ± 55.81 nm, PDI 0.201 ± 0.00 and zeta potential − 17.2 ± 2.35 mV. The particle size is very much similar to the predicted value of optimized CNL by the statistical design software. The PDI 0.201 indicated nearly monodispersed particles with little variation in size distribution. It also confirms minimum aggregation or agglomeration among the particles [46]. The desirable range of PDI for pharmaceutical nanoparticulate systems is < 0.3, and most of the previously reported NLC lies in this range only [47,48]. The zeta potential is used to analyze the charge on the surface of the nanocarrier and thus to predict its stability. The optimized curcumin-loaded NLC was noted with zeta potential − 17.2 ± 2.35 mV. The negative lower values of zeta potential accredited for electrostatically stable particles in the colloidal system. It has already been reported that a zeta potential near − 20 mV attributed to the physical stability of the system [49,50]. Also, the negative charge on the surface of the prepared CNL was found safe for human application and suitable for intranasal administration in future studies [51].

3.5. Scanning electron microscopy

Morphological features of lyophilized CNL were studied by scanning electron microscope (SEM, JSM-6010LA, JEOL Ltd., Tokyo). The SEM micrographs of the optimized formulation evident almost uniform-sized, spherical particles of NLC. Fig. 5(a) showed flakes like structure which indicated the lumps/ aggregated of lyophilized NLC formed due to drying and storage of the prepared formulation upon lyophilization. Small amount of lyophilized sample was ultrasonicated to assure the uniform distribution of individual particles and analyzed again. Fig. 5(b) and (c) showed the surface behavior of homogenously dispersed NLC particles which were small, almost spherical, uniform-sized particles with a size range below 200 nm at different magnifications x2700 and x3700, respectively. Fig. 5(d) clearly demonstrated the outer surface of the NLC as nearly spherical and uneven or imperfect porous surface, which is the characteristic and desirable property of NLC to facilitate

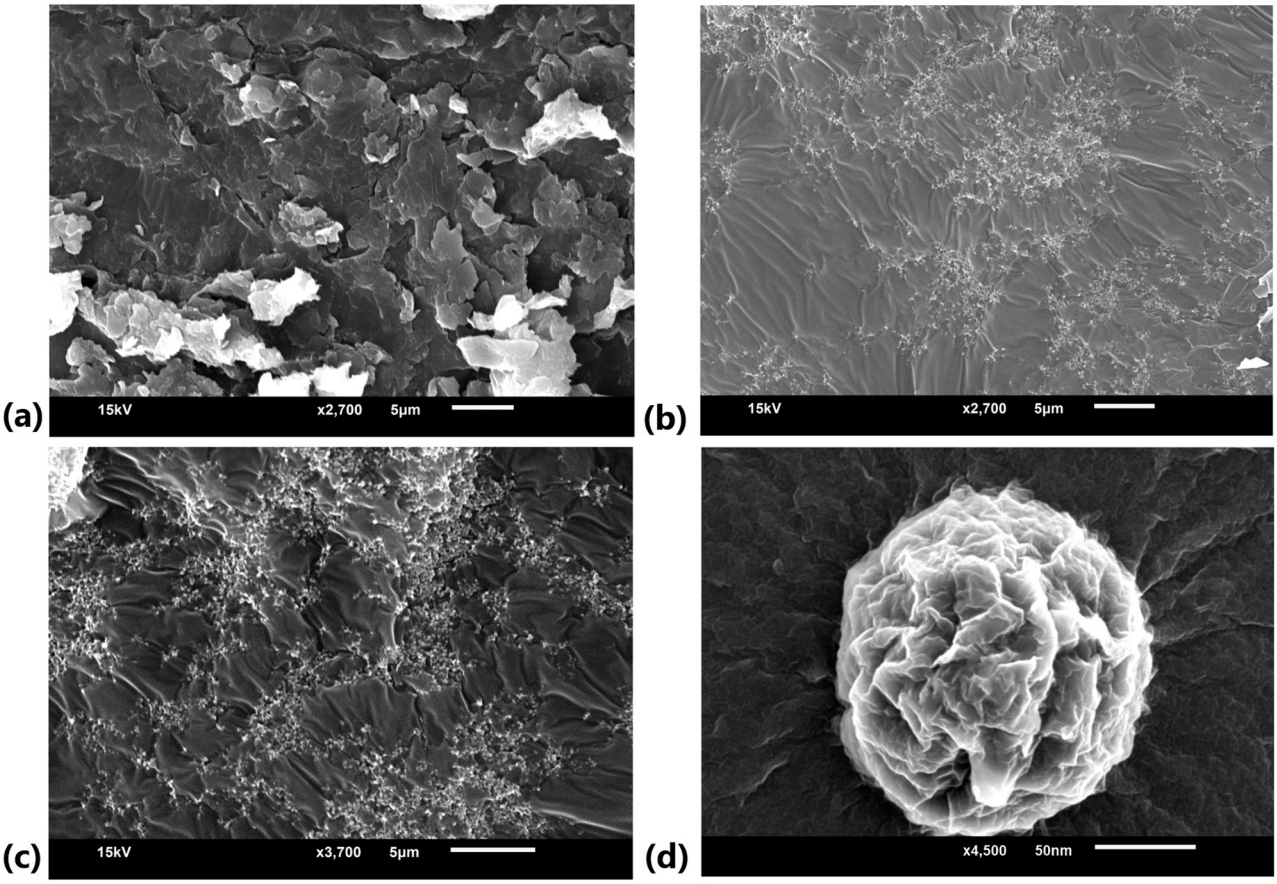

Fig. 5. (a) SEM image of lyophilized curcumin loaded NLC, which shows aggregates of dried formulation at 2700x. (b) & (c) SEM micrographs of lyophilized curcumin loaded NLC upon ultrasonication for proper dispersion at different magnifications. Micrograms showed mostly uniform and spherical particles of drug loaded NLC (b) at lower magnification 2700x and (c) at higher magnification 3700x, and (d) nearly spherical in shape, uneven, imperfect and porous surface structure of the prepared NLC formulation.

higher drug entrapment. Such surface behavior aligned to the reported concept of NLC structure that imperfect arrangement of solid and liquid lipid enhances the drug entrapment efficiency compared to other lipid nanocarrier systems [34]. The size observed from the micrograph was less than 150 nm which almost align with our finding by dynamic light scattering and predicted value by the software.

3.6. Entrapment efficiency

Entrapment efficiency of different CNL formulations ranges from 66.09–93.70%. The variation in percent entrapment efficiency of different prepared formulations attributed to various formulation variables, including solid and liquid lipid content. An increase in entrapment efficiency was observed with increasing concentration of Compritol® 888 while the formulation with highest ratio of solid/liquid lipid (80:20) showed a comparative decrease than the middle (75:25) combination. Such results might be due to decreased liquid lipid content in the formulation, which is supposed to maintain the irregular arrangement of solid lipid matrix and facilitate more drug entrapment inside [34]. Previous studies also reported Compitol® 888 promotes drug entrapment in the NLC because of the higher mono-, di- and tri- glyceride content, which facilitates solubilization of drug in lipid. Additionally, the liquid lipid acts in synergy and makes sufficient space for drug entrapment [52]. Hence, we predict that a perfect combination of solid and liquid lipid provides best range of drug entrapment. Another critical factor is the recrystallization of solid lipid, which causes expulsion of the entrapped drug during cooling process. The addition of suitable liquid lipid (Captex® 355) prevents the drug expulsion during recrystallization by facilitating the formation of a less ordered crystalline structure or amorphous NLC and ensuring the higher loading [53]. We also observed that the formulation subjected for ultrasonication immediately after melt emulsification showed an initial increase followed by a decrease in drug entrapment efficiency with further increase in sonication time. Thus, we predicted that ultrasonication time also has a considerable impact on entrapment efficiency and may prevent the expulsion of initially entrapped drug from the lipid crystals [54]. Besides, it remains unaffected by the surfactant concentration. All the CNL (from CNL1 to CNL32) found to have drug entrapment efficiency in the acceptable range (> 75%), although the formulations were having a percentage entrapment efficiency of more than 80% are considered best. The % drug entrapment and % drug loading efficiency of the optimized formulations were noted as 92.74 ± 0.27% and 1.87 ± 0.01%.

3.7. In vitro drug release study

The drug release study demonstrated a biphasic release of the drug from the optimized CNL formulation. An initial burst release of around 20.7 ± 0.01% drug was observed in the first 2 h followed by slow and prolonged release of up to 92.73 ± 0.06% drug up to 48 h. On the other hand, the curcumin solution showed immediate release of 89.38% of the drug only in first hour and almost all the drug content released in 4 h. The later slow release from the solution might be due to the lack of concentration gradient between donor and receptor compartment. The biphasic release behavior of NLC might be due to the imperfect arrangement of the solid and liquid lipid blend of the NLC. The drug embedded in the solid lipid crystals might provide slow and prolonged release, while the immediate release could be attributed to the drug present in the liquid lipid. Some drug might also present in the outer shell as free moiety, which also contributed to the burst release in the first 2 h. The drug release profile of CNL in comparison with drug solution is shown in Fig. 6.

3.7.1. Release kinetics assessment

The drug release profile of the optimized CNL formulation was valuated through different kinetic models using DDSolver 1.0 to assess the drug release kinetics. The release data was fitted to the kinetic equations of zero-order, first-order, Higuchi, Korsmeyer-Peppas, Hixson-Crowell and Weibull model. The best-fitted model was judged by the goodness of fit parameters like coefficient of determination (R^2), adjusted coefficient of determination (R^2_adj), Akaike information criterion (AIC) and model selection criterion (MSC). Based on the values of R^2, R^2_adj (near to 1), AIC (minimum) and MSC (maximum), the release behavior of CNL could be best explained by the Weibull kinetic model (Table 4). As per the literature, Weibull model is also best suited to describe the release profile of drug from the matrix-based drug delivery system. The release mechanism was predicted by the exponent (β) of the mathematical model (Weibull equation). In our study, β value was noted 0.766, which lies in the range of 0.75–1.0, indicate a combined drug release mechanism. Together the analysis of complete set of data through power law and the Weibull function gave further details about

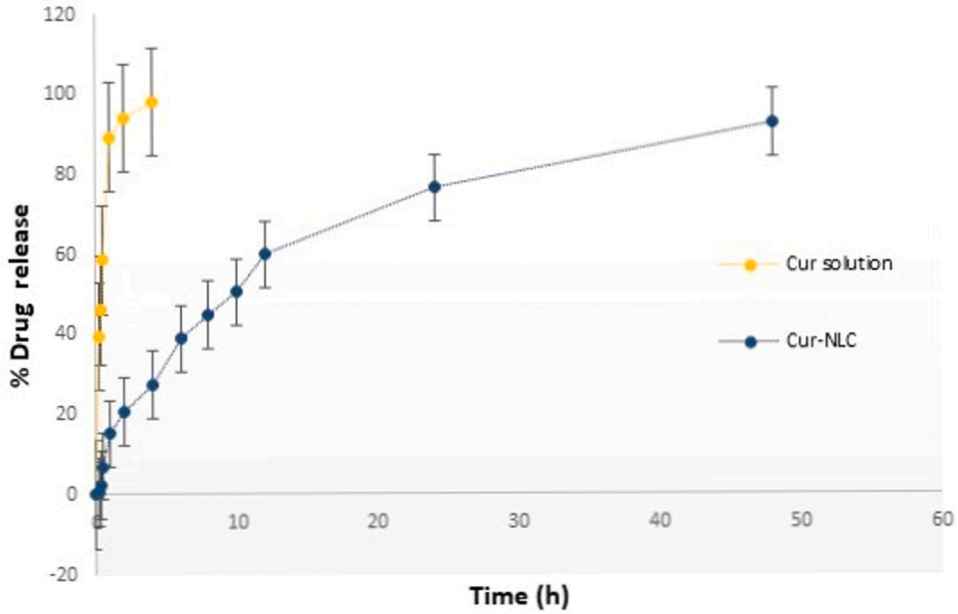

Fig. 6. *In vitro* release profile of Cur from plain drug solution and CNL for 48 h in physiological medium (phosphate buffer pH 7.4) at 37 ℃.

Table 4
In vitro release kinetics parameters of prepared CNL formulation.

Parameters	Zero order	First order	Higuchi	Korsmeyer-Peppas	Hixson-Crowell	Weibull
R^2	0.5877	0.9813	0.9725	0.9747	0.9627	**0.9958**
R^2_adj	0.5877	0.9813	0.9725	0.9724	0.9627	**0.9950**
AIC	111.3513	71.1106	76.1605	77.0536	80.1310	55.6333
MSC	0.6227	3.7182	3.3297	3.2610	3.0243	4.9087
Best fit values	k0: 2.550	k1: 0.074	kH: 14.769	kKP: 16.140 n: 0.470	kHC: 0.022	α: 7.838 β: 0.766 Ti: 0.097

n: diffusional exponent in demonstrating mechanism of drug release
α, β & Ti: exponents of Weibull model

the release mechanism [55,56]. α-value was found at 7.838, which represents the time dependant release pattern. At the same time, n value (0.47) from the Korsmeyer-Peppas equation confirms the drug release from the lipid matrix followed Fickian diffusion. Another mechanism might be surface erosion, responsible for initial burst release. β value less than < 1 elucidates a steeper increase of the release mechanism. Similar release behavior was also observed in a previous study by Meng et al. [57], claimed combined release behavior as a function of Weibull equation exponent β and n value by Korsmeyer-Peppas equation.

3.8. Stability studies

Accelerated stability study of the prepared formulation was performed in terms of physical appearance, particle size and drug entrapment efficiency upon storage in different conditions as per the ICH guidelines Q1A. The formulation was observed at different time intervals, as mentioned above. No significant change in the physical appearance of the CNL was observed at both the regular and accelerated conditions of temperature and humidity. A little increase in particle size and decrease in entrapment efficiency was recorded after 3 months of storage at both conditions. The changes were slightly higher in accelerated conditions than the regular condition (Table 5). Although the changes were not as significant to be considered and thus it can be concluded that the optimized formulation was satisfactorily stable during the entire period.

Table 5
Accelerated stability study of IN CNL as per ICH guideline.

Time (month)	25 ± 2 ℃ and 60 ± 5% RH			40 ± 2 ℃ and 75 ± 5% RH		
	Change in Physical appearance	Particle size (nm)	% EE	Change in Physical appearance	Particle size (nm)	% EE
0	No	121.8	93.95	No	121.8	93.95
1	No	121.93	93.17	No	122.04	92.47
3	No	125.37	91.38	No	129.61	90.25

4. Conclusion

The present study demonstrated the design and optimization of curcumin-loaded NLC further intended for the treatment of AD. The drug-loaded NLC was successfully prepared by modified melt-emulsification method followed by ultrasonication, and experimental design and optimization were done by response surface methodology using Box-Behnken design. The study aimed to optimize the formulation variables and design a cost-effective, biodegradable and stable nanocarrier with higher drug entrapment and sustained release profile. The optimized formulation demonstrated particle size 121.8 nm, which lies in the acceptable range for brain delivery and is supposed to promote cell permeation upon intranasal administration. At the same time, we found higher entrapment efficiency (92.74%) and a higher drug release profile with an initial burst and subsequent sustained release of 92.73%. The drug release follows the Weibull kinetic equation with a steeper type release curve and a combined drug release mechanism, including Fickian diffusion, explained by the exponent function β and n of the kinetic models. The results of preliminary studies illustrated that prepared NLC fulfills the desired characteristics of nanocarrier for brain delivery and will be further developed as *in situ* gel for intranasal administration. The system will also be evaluated for the anti-AD potency of the encapsulated drug.

Funding support

None.

CRediT authorship contribution statement

Mukta Agrawal: Writing - original draft, Methodology, Software. **Shailendra Saraf:** Conceptualization. **Madhulika Pradhan:** Revision. **Ravish J Patel:** Resources. **Gautam Singhvi:** Formal analysis. **Ajazuddin:** Supervision. **Amit Alexander:** Conceptualization, Visualization, Supervision.

Conflict of interest statement

None.

Acknowledgment

The author wants to thank National Institute of Pharmaceutical Education and Research, Guwahati (NIPER-Guwahati), India and Department of Pharmaceutics, Raman Bhai Patel College of Pharmacy, CHARUSAT, Gujarat, India for providing infrastructural facilities. The authors are also grateful to the Department of Pharmacy, Birla Institute of Technology and Science, Pilani, India for analytical support. Last but not the least, the authors would also like to thank Gattefosse India Pvt. Ltd. for providing gift samples.

References

[1] M. Agrawal, S. Saraf, S. Saraf, S.G. Antimisiaris, M.B. Chougule, S.A. Shoyele, A. Alexander, Nose-to-brain drug delivery: an update on clinical challenges and progress towards approval of anti-Alzheimer drugs, J. Control. Release 281 (2018) 139–177.
[2] M. Agrawal, Ajazuddin, D.K. Tripathi, S. Saraf, S. Saraf, S.G. Antimisiaris, S. Mourtas, M. Hammarlund-Udenaes, A. Alexander, Recent advancements in liposomes targeting strategies to cross blood-brain barrier (BBB) for the treatment of Alzheimer's disease, J. Control. Release 260 (2017) 61–77.
[3] M. Agrawal, S. Saraf, S. Saraf, S.G. Antimisiaris, N. Hamano, S.D. Li, M. Chougule, S.A. Shoyele, U. Gupta, Ajazuddin, A. Alexander, Recent advancements in the field of nanotechnology for the delivery of anti-Alzheimer drug in the brain region, Expert Opin. Drug Deliv. 15 (6) (2018) 589–617.
[4] S. Sadegh Malvajerd, Z. Izadi, A. Azadi, M. Kurd, H. Derakhshankhah, M. Sharifzadeh, H. Akbari Javar, M. Hamidi, Neuroprotective potential of curcumin-loaded nanostructured lipid carrier in an animal model of Alzheimer's disease: behavioral and biochemical evidence, J. Alzheimer's Dis. 69 (3) (2019) 671–686.
[5] WHO, Demetia, Fact Sheets, World Health Organization, (2020).
[6] A. Alexander, S. Saraf, Nose-to-brain drug delivery approach: a key to easily accessing the brain for the treatment of Alzheimer's disease, Neural Regen. Res. 13 (12) (2018) 2102–2104.

[7] T.T. Nguyen, T.T.D. Nguyen, T.K.O. Nguyen, T.K. Vo, V.G. Vo, Advances in developing therapeutic strategies for Alzheimer's disease, Biomed. Pharmacother. 139 (2021), 111623.
[8] M. Agrawal, S. Saraf, S. Saraf, S.K. Dubey, A. Puri, U. Gupta, P. Kesharwani, V. Ravichandiran, P. Kumar, V.G.M. Naidu, U.S. Murty, Ajazuddin, A. Alexander, Stimuli-responsive In situ gelling system for nose-to-brain drug delivery, J. Control. Release 327 (2020) 235–265.
[9] K. Bisht, K. Sharma, M.-È. Tremblay, Chronic stress as a risk factor for Alzheimer's disease: roles of microglia-mediated synaptic remodeling, inflammation, and oxidative stress, Neurobiol. Stress 9 (2018) 9–21.
[10] M. Saeedi, A. Rashidy-Pour, Association between chronic stress and Alzheimer's disease: therapeutic effects of Saffron, Biomed. Pharmacother. 133 (2021), 110995.
[11] L. Cassidy, F. Fernandez, J.B. Johnson, M. Naiker, A.G. Owoola, D.A. Broszczak, Oxidative stress in alzheimer's disease: a review on emergent natural polyphenolic therapeutics, Complement. Ther. Med. 49 (2020), 102294.
[12] S.K. Dubey, K.K. Lakshmi, K.V. Krishna, M. Agrawal, G. Singhvi, R.N. Saha, S. Saraf, S. Saraf, R. Shukla, A. Alexander, Insulin mediated novel therapies for the treatment of Alzheimer's disease, Life Sci. 249 (2020), 117540.
[13] A. Alexander, S. Saraf, Nose-to-brain drug delivery approach: a key to easily accessing the brain for the treatment of Alzheimer's disease, Neural Regen. Res 13 (12) (2018) 2102–2104.
[14] M. Agrawal, E. Prathyusha, H. Ahmed, S.K. Dubey, P. Kesharwani, G. Singhvi, V.G. M. Naidu, A. Alexander, Biomaterials in treatment of Alzheimer's disease, Neurochem. Int. 145 (2021), 105008.
[15] P. Anand, A.B. Kunnumakkara, R.A. Newman, B.B. Aggarwal, Bioavailability of curcumin: problems and promises, Mol. Pharm. 4 (6) (2007) 807–818.
[16] G.R. Vaz, G. Hädrich, J. Bidone, J.L. Rodrigues, M.C. Falkembach, J.L. Putaux, M. A. Hort, J.M. Monserrat, A.S. Varela Junior, H.F. Teixeira, A.L. Muccillo-Baisch, A. P. Horn, C.L. Dora, Development of nasal lipid nanocarriers containing curcumin for brain targeting, J. Alzheimer's Dis. 59 (3) (2017) 961–974.
[17] M. Nasr, Development of an optimized hyaluronic acid-based lipidic nanoemulsion co-encapsulating two polyphenols for nose to brain delivery, Drug Deliv. 23 (4) (2016) 1444–1452.
[18] R. Giacomeli, J.C. Izoton, R.B. dos Santos, S.P. Boeira, C.R. Jesse, S.E. Haas, Neuroprotective effects of curcumin lipid-core nanocapsules in a model Alzheimer's disease induced by β-amyloid 1-42 peptide in aged female mice, Brain Res. 1721 (2019), 146325.
[19] A. Eftekhari, S.M. Dizaj, L. Chodari, S. Sunar, A. Hasanzadeh, E. Ahmadian, M. Hasanzadeh, The promising future of nano-antioxidant therapy against environmental pollutants induced-toxicities, Biomed. Pharmacother. 103 (2018) 1018–1027.
[20] N. Ahmadi, M.-J. Hosseini, K. Rostamizadeh, M. Anoush, Investigation of therapeutic effect of curcumin α and β glucoside anomers against Alzheimer's disease by the nose to brain drug delivery, Brain Res. 2021 (1766), 147517.
[21] Rabima, A. Oktamauri, Characterisation and cytotoxicity assay of curcumin nanostructured lipid carrier on HeLa cells, IOP Conf. Ser. Earth Environ. Sci. 667 (1) (2021), 012055.
[22] D.E. Igartúa, C.S. Martinez, Sd.V. Alonso, N.S. Chiaramoni, M.J. Prieto, Toxicity assessment of free and dendrimer-complexed curcumin in zebrafish larvae, PharmaNutrition 13 (2020), 100201.
[23] M. Saeedi, M. Eslamifar, K. Khezri, S.M. Dizaj, Applications of nanotechnology in drug delivery to the central nervous system, Biomed. Pharmacother. 111 (2019) 666–675.
[24] A. Alexander, M. Agrawal, A. Uddin, S. Siddique, A.M. Shehata, M.A. Shaker, S. Ata Ur Rahman, M.I.M. Abdul, M.A. Shaker, Recent expansions of novel strategies towards the drug targeting into the brain, Int. J. Nanomed. 14 (2019) 5895–5909.
[25] O. Gartziandia, S.P. Egusquiaguirre, J. Bianco, J.L. Pedraz, M. Igartua, R. M. Hernandez, V. Préat, A. Beloqui, Nanoparticle transport across in vitro olfactory cell monolayers, Int. J. Pharm. 499 (1–2) (2016) 81–89.
[26] K.V. Krishna, G. Wadhwa, A. Alexander, N. Kanojia, R.N. Saha, R. Kukreti, G. Singhvi, S.K. Dubey, Design and biological evaluation of lipoprotein-based donepezil nanocarrier for enhanced brain uptake through oral delivery, ACS Chem. Neurosci. 10 (9) (2019) 4124–4135.
[27] R.G. Madane, H.S. Mahajan, Curcumin-loaded nanostructured lipid carriers (NLCs) for nasal administration: design, characterization, and in vivo study, Drug Deliv. 23 (4) (2016) 1326–1334.
[28] A. Khosa, S. Reddi, R.N. Saha, Nanostructured lipid carriers for site-specific drug delivery, Biomed. Pharmacother. 103 (2018) 598–613.
[29] H. Barabadi, H. Vahidi, K. Damavandi Kamali, M. Rashedi, O. Hosseini, M. Saravanan, Emerging theranostic gold nanomaterials to combat colorectal cancer: a systematic review, J. Clust. Sci. 31 (4) (2020) 651–658.
[30] N. Naseri, H. Valizadeh, P. Zakeri-Milani, Solid lipid nanoparticles and nanostructured lipid carriers: structure, preparation and application, Adv. Pharm. Bull. 5 (3) (2015) 305–313.
[31] A. Alexander, M. Agrawal, S. Saraf, S. Saraf, Ajazuddin, M.B. Chougule, Formulation strategies of nano lipid carrier for effective brain targeting of anti-AD drugs, Curr. Pharm. Des. 26 (2020) 3269–3280.
[32] M. Pradhan, A. Alexander, M.R. Singh, D. Singh, S. Saraf, S. Saraf, Ajazuddin, Understanding the prospective of nano-formulations towards the treatment of psoriasis, Biomed. Pharmacother. 107 (2018) 447–463.
[33] S.N. Kanojia N, N. Gupta, S. Singh, Applications of nanostructured lipid carriers: recent advancements and patent review, Biointerface Res. Appl. Chem. 12 (1) (2021) 638–652.
[34] M. Agrawal, S. Saraf, S. Saraf, S.K. Dubey, A. Puri, R.J. Patel, Ajazuddin, V. Ravichandiran, U.S. Murty, A. Alexander, Recent strategies and advances in the fabrication of nano lipid carriers and their application towards brain targeting, J. Control. Release 321 (2020) 372–415.
[35] D.G. Gadhave, C.R. Kokare, Nanostructured lipid carriers engineered for intranasal delivery of teriflunomide in multiple sclerosis: optimization and in vivo studies, Drug Dev. Ind. Pharm. 45 (5) (2019) 839–851.
[36] V. Pokharkar, A. Patil-Gadhe, P. Palla, Efavirenz loaded nanostructured lipid carrier engineered for brain targeting through intranasal route: in-vivo pharmacokinetic and toxicity study, Biomed. Pharmacother. 94 (2017) 150–164.
[37] L. Mandpe, A. Kyadarkunte, V. Pokharkar, Assessment of novel iloperidone and idebenone-loaded nanostructured lipid carriers: brain targeting efficiency and neuroprotective potential, Ther. Deliv. 4 (11) (2013) 1365–1383.
[38] I. Jazuli, Annu, B. Nabi, T. Moolakkadath, T. Alam, S. Baboota, J. Ali, Optimization of nanostructured lipid carriers of lurasidone hydrochloride using box-behnken design for brain targeting: in vitro and in vivo studies, J. Pharm. Sci. 108 (9) (2019) 3082–3090.
[39] P. Kumar, G. Sharma, R. Kumar, B. Singh, R. Malik, O.P. Katare, K. Raza, Promises of a biocompatible nanocarrier in improved brain delivery of quercetin: biochemical, pharmacokinetic and biodistribution evidences, Int. J. Pharm. 515 (1–2) (2016) 307–314.
[40] A. Anand, M. Arya, G. Kaithwas, G. Singh, S.A. Saraf, Sucrose stearate as a biosurfactant for development of rivastigmine containing nanostructured lipid carriers and assessment of its activity against dementia in C. elegans model, J. Drug Deliv. Sci. Technol. 49 (2019) 219–226.
[41] P.R. Wavikar, P.R. Vavia, Rivastigmine-loaded in situ gelling nanostructured lipid carriers for nose to brain delivery, J. Liposome Res. 25 (2) (2015) 141–149.
[42] G. Shevalkar, P. Vavia, Solidified nanostructured lipid carrier (S-NLC) for enhancing the oral bioavailability of ezetimibe, J. Drug Deliv. Sci. Technol. 53 (2019), 101211.
[43] Y.M. Gabal, A.O. Kamel, O.A. Sammour, A.H. Elshafeey, Effect of surface charge on the brain delivery of nanostructured lipid carriers in situ gels via the nasal route, Int. J. Pharm. 473 (2014) 442–457.
[44] C. Thapa, A. Ahad, M. Aqil, S.S. Imam, Y. Sultana, Formulation and optimization of nanostructured lipid carriers to enhance oral bioavailability of telmisartan using Box–Behnken design, J. Drug Deliv. Sci. Technol. 44 (2018) 431–439.
[45] A. Qadir, M. Aqil, A. Ali, M.H. Warsi, M. Mujeeb, F.J. Ahmad, S. Ahmad, S. Beg, Nanostructured lipidic carriers for dual drug delivery in the management of psoriasis: systematic optimization, dermatokinetic and preclinical evaluation, J. Drug Deliv. Sci. Technol. 57 (2020), 101775.
[46] T. Mudalige, H. Qu, D. Van Haute, S.M. Ansar, A. Paredes, T. Ingle, Chapter 11 - characterization of nanomaterials: tools and challenges, in: A. López Rubio, M. J. Fabra Rovira, M. martínez Sanz, L.G. Gómez-Mascaraque (Eds.), Nanomaterials for Food Applications, Elsevier, 2019, pp. 313–353.
[47] M. Fang, Y. Jin, W. Bao, H. Gao, M. Xu, D. Wang, X. Wang, P. Yao, L. Liu, In vitro characterization and in vivo evaluation of nanostructured lipid curcumin carriers for intragastric administration, Int. J. Nanomed. 7 (2012) 5395–5404.
[48] S. Bashiri, B. Ghanbarzadeh, A. Ayaseh, J. Dehghannya, A. Ehsani, Preparation and characterization of chitosan-coated nanostructured lipid carriers (CH-NLC) containing cinnamon essential oil for enriching milk and anti-oxidant activity, LWT 119 (2020), 108836.
[49] A. Khan, S.S. Imam, M. Aqil, A. Ahad, Y. Sultana, A. Ali, K. Khan, Brain targeting of temozolomide via the intranasal route using lipid-based nanoparticles: brain pharmacokinetic and scintigraphic analyses, Mol. Pharm. 13 (11) (2016) 3773–3782.
[50] S.S. Salunkhe, N.M. Bhatia, M.S. Bhatia, Implications of formulation design on lipid-based nanostructured carrier system for drug delivery to brain, Drug. Deliv. 23 (4) (2016) 1306–1316.
[51] D. Gadhave, H. Choudhury, C. Kokare, Neutropenia and leukopenia protective intranasal olanzapine-loaded lipid-based nanocarriers engineered for brain delivery, Appl. Nanosci. 9 (2018).
[52] H. Abbas, H. Refai, N. El Sayed, Superparamagnetic iron oxide-loaded lipid nanocarriers incorporated in thermosensitive in situ gel for magnetic brain targeting of clonazepam, J. Pharm. Sci. 107 (8) (2018) 2119–2127.
[53] S. Swidan, H. Ghonaim, A. Ahmed, M. Ghorab, Comparative study of solid lipid nanoparticles and nanostructured lipid carriers for in vitro Paclitaxel delivery, J. Chem. Pharm. Res. 2016 (2016) 482–493.
[54] Y. He, L. Luo, S. Liang, M. Long, H. Xu, Influence of probe-sonication process on drug entrapment efficiency of liposomes loaded with a hydrophobic drug, Int. J. Polym. Mater. 68 (4) (2019) 193–197.
[55] V. Papadopoulou, K. Kosmidis, M. Vlachou, P. Macheras, On the use of the Weibull function for the discernment of drug release mechanisms, Int. J. Pharm. 309 (1) (2006) 44–50.
[56] C. Ferreira da Silva, P. Severino, F. Martins, M.H.A. Santana, E.B. Souto, Didanosine-loaded chitosan microspheres optimized by surface-response methodology: a modified "Maximum Likelihood Classification" approach formulation for reverse transcriptase inhibitors, Biomed. Pharmacother. 70 (2015) 46–52.
[57] F. Meng, S. Asghar, Y. Xu, J. Wang, X. Jin, Z. Wang, J. Wang, Q. Ping, J. Zhou, Y. Xiao, Design and evaluation of lipoprotein resembling curcumin-encapsulated protein-free nanostructured lipid carrier for brain targeting, Int. J. Pharm. 506 (1) (2016) 46–56.